Chinese Chemical Letters 36 (2025) 110192

Contents lists available at ScienceDirect

Chinese Chemical Letters

journal homepage: www.elsevier.com/locate/cclet

Improved hydrogen and oxygen evolution rates in Pt@TiO_2@RuO_2 hollow nanoshells through dielectric Mie resonance and spatial cocatalyst separation

Xiaxi Yao[a], Xiuli Hu[a], Fangcheng Huang[d,*], Xuhong Wang[a], Xuekun Hong[b,*], Dawei Wang[c,*]

[a] School of Materials Engineering, Changshu Institute of Technology, Changshu 215500, China
[b] School of Electronic Information Engineering, Changshu Institute of Technology, Changshu 215500, China
[c] Key Laboratory of Integrated Regulation and Resource Development on Shallow Lake of Ministry of Education, College of Environment, Hohai University, Nanjing 210098, China
[d] Department of Information Engineering, Electronics, and Telecommunications, Sapienza University of Rome, Piazzale Aldo Moro 5, 00185 Roma, Italy

ARTICLE INFO

Article history:
Received 8 March 2024
Revised 10 June 2024
Accepted 27 June 2024
Available online 29 June 2024

Keywords:
Dielectric Mie resonance
Hollow nanoshells
Spatial charge separation
Overall water splitting
Photocatalysis

ABSTRACT

Photocatalytic overall water splitting is a promising method for producing clean hydrogen energy, but faces challenges such as low light utilization efficiency and high charge carrier recombination rates. This study demonstrates that dielectric Mie resonance in TiO_2 hollow nanoshells can enhance electric field intensity and increase light absorption through resonant energy transfer, compared to crushed TiO_2 nanoparticles. The Mie resonance effect was confirmed through fluorescence spectra, photo-response current measurements, photocatalytic water splitting experiments, and Mie calculation. The incident electric-field amplitude was doubled in hollow nanoshells, allowing for increased light trapping. Additionally, the spatially separated Pt and RuO_2 cocatalysts on the inner and outer surfaces facilitated the separation of photoinduced electrons and holes. Pt@TiO_2@RuO_2 hollow nanoshells exhibited superior photocatalytic water splitting performance, with a stable H_2 generation rate of 50.1 μmol g^{-1} h^{-1} and O_2 evolution rate of 25.1 μmol g^{-1} h^{-1}, outperforming other nanostructures such as TiO_2, Pt@TiO_2, and TiO_2@RuO_2 hollow nanoshells. This study suggests that dielectric Mie resonance and spatially-separated cocatalysts offer a new approach to simultaneously enhance light absorption and charge carrier transfer in photocatalysis.

Photocatalytic overall water splitting is considered an efficient strategy to address the energy crisis, utilizing solar light as the sole energy source and pure water as the reactant. Significant progress has been made by various research groups over the past decades, although the work mainly remains in the laboratory phase [1–3]. Two major challenges must be overcome before practical industrial application. The first challenge involves improving sunlight utilization efficiency, typically achieved through strategies such as element doping, sensitization, or composites to broaden the photocatalyst's photo-response range across the solar energy spectrum [4–6]. Factors like doping elements and concentration, sensitizer stability and cost, and the alignment of valence and conduction band potentials must be carefully studied for optimal catalytic performance. Moreover, a considerable amount of incident light passes through the photocatalytic dispersion system without converting into excited charge carriers. Plasmonic nanostructures have been developed to enhance light absorption through the nanoantenna effect and improved electric-field distribution due to localized surface plasmonic resonance (LSPR) of noble metal nanoparticles [7–9]. The frequency of LSPR is influenced by factors such as composition, size, geometry, dielectric environment, and nanoparticle separation distance. However, these structures often face challenges such as energy loss and excessive heat generation, limiting their potential benefits for photocatalysis. Whispering gallery modes (WGMs) in dielectric spheres have recently gained attention due to their low loss, stability, and resonance tunability. WGMs arise from the continuous reflection of incident light within the optical cavity, confining and guiding light along the surface [10–12]. Specifically, constructive resonance mode, known as Mie resonance, occurs when the light path corresponds to a multiple of a specific wavelength inside the sphere, resulting in an enhancement of the electric and magnetic field intensity [13–

* Corresponding authors.
E-mail addresses: fangcheng.huang@uniroma1.it (F. Huang), xkhong@cslg.edu.cn (X. Hong), dawei.wang@hhu.edu.cn (D. Wang).

https://doi.org/10.1016/j.cclet.2024.110192
1001-8417/

16]. The resonance wavelength in hollow nanoshells is dependent on inner diameter, shell thickness, refractive index of shell materials, and surrounding medium [17]. Dielectric Mie resonance offers the potential to rival or complement plasmonic resonances, and not only shares properties with LSPR, such as enhanced scattering, but also features unique characteristics like strong magnetic resonance. This enhancement of electromagnetic field has been utilized by various research groups to enhance light absorption in thin-film solar cells, by directing the confined light within resonant spheres into absorbing materials to improve light trapping capabilities [15,18,19]. Successful light trapping enhancement hinges on tuning the resonance wavelength to align with the photo-response range of semiconductors. While Mie resonance in silica hollow spheres has shown promise for structural colors [20–22], semiconductor materials are more commonly used in different fields like photocatalysis, photovoltaics, and sensors. Our previous work focused on exploring Mie resonance in TiO_2 hollow nanoshells, demonstrating the ability to modulate resonant peaks by adjusting the inner diameter or surrounding medium [23]. Additionally, we showcased an anti-counterfeiting application by changing the structural color reversibly to reveal hidden information in designed patterns. Building on the concept of plasmonic resonance in noble metals for photocatalysis, we studied Mie resonance in TiO_2 nanoshells for photocatalytic hydrogen evolution, aiming to enhance the light absorption. Matching the resonance wavelength of TiO_2 hollow nanoshells with the absorption range of sensitized dye or CdS semiconductor significantly improved photocatalytic performance, highlighting the potential of Mie resonance-enhanced light trapping in dielectric hollow spheres [24,25].

The acceleration of photogenerated charge carriers' separation is another challenge in enhancing overall water splitting efficiency. Various strategies have been explored to facilitate the movement of electron-hole pairs and reduce recombination rates, such as adjusting particle size, controlling crystal orientation, creating Z-scheme and S-scheme structures, and loading cocatalysts [26–29]. Among these approaches, cocatalysts with spatial separation play a crucial role in directing electrons and holes along different paths, minimizing contact opportunities during migration from bulk to surface, and thereby suppressing recombination of charge carriers. Hollow nanostructured materials, known for their large surface area, specific space, low density, and high loading capacity, have been extensively studied in catalysis, energy storage, and drug delivery [30–32]. The inner cavities and outer surfaces of these materials offer naturally segregated regions for the incorporation of reduction and oxidation cocatalysts.

Herein, hollow TiO_2 microspheres were synthesized with spatially-separated Pt and RuO_2 cocatalysts for dielectric Mie resonance-enhanced photocatalytic water splitting. Pt and RuO_2 nanoparticles were positioned on the inner space and outer shell of the microspheres, respectively. Our previous work researched the dielectric Mie resonance in TiO_2 hollow nanoshells to match with another visible-light-response materials (dye or CdS) [24,25]. This study focuses on demonstrating that a single metal oxide semiconductor, specifically TiO_2, can exhibit dielectric Mie resonance and catalyze photocatalytic redox reactions. By leveraging dielectric Mie resonance in UV light, we aim to improve the light absorption capacity of TiO_2 hollow nanoshells. Experimental data, including fluorescence spectra, photo-response current, and photocatalytic hydrogen production, confirmed the presence of Mie resonance in the hollow nanoshells. Mie calculations indicated a twofold increase in near electric-field intensity. The photocatalytic results suggested that Pt@TiO_2@RuO_2 hollow nanoshells showed the highest hydrogen and oxygen evolution rates from overall water splitting, owing to the dual functionality of dielectric Mie resonance and charge separation.

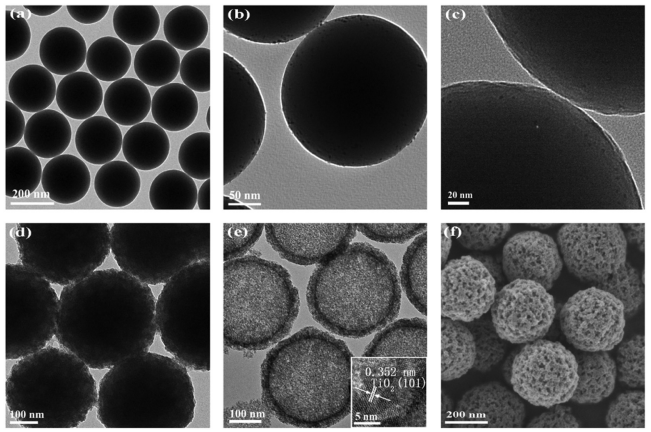

Fig. 1. (a-e) TEM images of samples at different stages of synthesizing Pt@TiO_2@RuO_2 hollow nanoshells, in order: (a) SiO_2 spheres, (b) SiO_2-Pt spheres, (c) SiO_2-Pt@SiO_2, (d) SiO_2-Pt@SiO_2@TiO_2, (e) Pt@TiO_2@RuO_2 hollow nanoshells and corresponding HRTEM image (inset). (f) SEM image of Pt@TiO_2@RuO_2 hollow nanoshells.

Pt@TiO_2@RuO_2 hollow nanoshells were prepared in a stepwise fashion to facilitate the movement of photoinduced electrons and holes in distinct directions. (see the detailed experiments in Supporting information). The microstructure of the synthesized samples at different stages was observed using transmission electron microscopy (TEM) (Fig. 1). The SiO_2 spheres exhibited monodispersion with an average diameter of 230 nm and a smooth surface (Fig. 1a). Small Pt nanoparticles (2.9 nm) were uniformly anchored on the outer surface of the SiO_2 spheres (Fig. 1b). Subsequently, one more SiO_2 layer coating was conducted to prevent Pt nanoparticles from migrating to the TiO_2 outer surface during subsequent calcination. TEM image further confirmed the positioning of Pt nanoparticles between the SiO_2 sphere and the SiO_2 coating layer (Fig. 1c), ensuring that the final Pt nanoparticles were located on the inner surface of TiO_2 hollow nanoshells. Rough TiO_2 shells were effectively coated on the outer SiO_2 surface through the hydrolysis of titanium *n*-butoxide (TBOT) (Fig. 1d). Following cation exchange, calcination, and complete etching, RuO_2 nanoparticles were anchored *in-situ* on the outer surface, and Pt@TiO_2@RuO_2 hollow nanoshells with an inner diameter of 260 nm and a shell thickness of 23 nm were produced (Fig. 1e). The high-resolution TEM (HRTEM) image in Fig. 1e inset displayed clear lattice fringes with a lattice distance of 0.352 nm, corresponding to the (101) facet of anatase TiO_2 [33,34]. RuO_2 nanoparticles were challenging to observe by TEM due to their small size and/or high distribution. The scanning electron microscopy (SEM) image in Fig. 1f further illustrated the formation of well-dispersed spherical particles. To investigate the distribution of Pt and RuO_2 in the hollow nanoshells, high-angle annular dark field scanning transmission electron microscopy (HAADF-STEM) and energy-dispersive X-ray spectroscopy (EDS) elemental mappings were performed (Fig. S1 in Supporting information). The Ti and O elements predominantly occupied the hollow structure with uniform dispersion, while Pt and Ru were dispersed on the inner and outer surfaces.

The phase structures of the synthesized samples were analyzed using powder X-ray diffraction (XRD). As presented in Fig. 2a, the TiO_2 hollow nanoshells displayed the anatase phase with characteristic diffraction peaks at 25.3°, 37.8°, 48.8°, 53.8°, 55.1°, and 62.7°, corresponding to (101), (004), (200), (105), (211), and (204) planes [35]. After loading Pt cocatalyst, another two small peaks at 39.7° and 46.2° were detected, which were attributed to (111) and (200) planes of cubic Pt [36]. Following ion exchange and calcination, the tetragonal RuO_2 phase was observed with weak

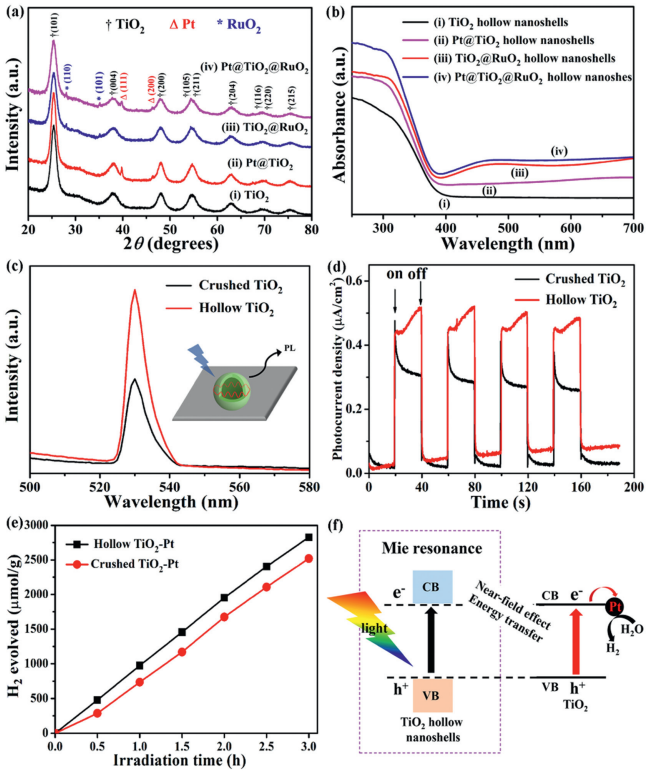

Fig. 2. (a) XRD patterns of TiO_2 hollow nanoshells, Pt@TiO_2 hollow nanoshells, TiO_2@RuO_2 hollow nanoshells, and Pt@TiO_2@RuO_2 hollow nanoshells prepared with 230 nm colloidal silica templates. (b) UV–vis diffused reflectance spectra of TiO_2, Pt@TiO_2, TiO_2@RuO_2, and Pt@TiO_2@RuO_2. (c) The photoluminescence (PL) spectra of hollow TiO_2 and crushed TiO_2 with an excitation wavelength of 360 nm. (d) Transient photocurrent response of the samples coated on ITO glass in 0.1 mol/L Na_2SO_4 aqueous solution at a bias of 0 V (*vs.* Ag/AgCl) during the switch on-off cycles every 20 s under simulated sunlight irradiation. (e) Photocatalytic hydrogen production from water splitting over hollow TiO_2 and crushed TiO_2 with 0.5% Pt under simulated sunlight irradiation. (f) Schematic illustration of dielectric Mie resonance-enhanced charge excitation.

diffraction peaks at 28.0° and 35.1° [37]. The Pt@TiO_2@RuO_2 hollow nanoshells presented the mixed phases of anatase TiO_2, cubic Pt, and tetragonal RuO_2, confirming the successful synthesis of hollow TiO_2 microspheres with spatially-separated Pt and RuO_2 co-catalysts. The crystalline size of anatase TiO_2 was calculated to be 7.0 nm according to the Scherrer's equation. UV–vis diffused reflectance spectra showed strong absorption below 400 nm for TiO_2 hollow nanoshells due to its band gap of 3.2 eV (Fig. 2b). Absorption in the UV region for Pt@TiO_2 and TiO_2@RuO_2 hollow nanoshells was attributed to anatase TiO_2, while absorption in the visible region was linked to Pt or RuO_2 nanoparticles. The Pt@TiO_2@RuO_2 hollow nanoshells exhibited significant absorption in both UV and visible regions. Plasmonic metal nanoparticles are known to transfer energy to nearby semiconductors through various mechanisms such as localized surface plasmonic resonance (LSPR) energy transfer, nanoantenna effect, or hot electron injection [38,39]. Similarly, the enhanced electric field from dielectric Mie resonance in hollow nanoshells can further excite the semiconductor, generating more electron-hole pairs when the resonance wavelength matches its intrinsic absorption range. Photoluminescence (PL) spectra serve as a strategy to confirm the presence of Mie resonance in hollow nanoshells. Both hollow TiO_2 and crushed TiO_2 exhibited anatase phase with identical nanoparticle size, as the crushed TiO_2 resulted from the structural collapse of hollow TiO_2 in an agate mortar. As described in Fig. 2c, both samples showed the emission peak at 530 nm with the excitation at 360 nm. The PL intensity of hollow TiO_2 was 1.90 times higher than that of crushed TiO_2, indicating that the confined incident light and dielectric Mie resonance in hollow nanoshells continuously excited charge carriers, resulting in more charge recombination and thus higher PL emission intensity [40,41]. Additionally, the transient photocurrent response was measured to evaluate the enhancement function of dielectric Mie resonance for light utilization (Fig. 2d). The photo-response current is a result of photoinduced electrons transferring within the TiO_2 semiconductor upon light irradiation [42]. This resonance effect in hollow nanoshells confines incident light around the surface, enhancing the excitation of electrons from the valence band to the conduction band of TiO_2. Consequently, an increased number of photogenerated electrons leads to higher photocurrent in TiO_2 hollow nanoshells during light exposure. In contrast, the photocurrent of TiO_2 nanoparticles slightly decreased under light illumination due to rapid recombination of charge carriers. To elucidate the enhancement of light utilization efficiency through dielectric Mie resonance, a photocatalytic hydrogen evolution experiment was conducted using hollow TiO_2 and crushed TiO_2 with a 0.5% Pt cocatalyst in the presence of a methanol sacrificial agent (Fig. 2e). The hollow TiO_2 catalyst showed the stable photocatalytic H_2 production with an evolution rate of 0.97 mmol g^{-1} h^{-1}, which was 1.24 times higher than that of crushed TiO_2 nanoparticles (0.78 mmol g^{-1} h^{-1}). Fig. 2f schematically illustrated the photocatalytic mechanism, involving dielectric Mie resonance and charge separation. Upon light irradiation, electrons in the TiO_2 semiconductor were excited and transferred to the Pt nanoparticles for photocatalytic hydrogen production. Furthermore, the dielectric Mie resonance boosted the electric field intensity and transferred energy to TiO_2, resulting in the generation of additional excited electrons. Consequently, dielectric Mie resonance proved advantageous in enhancing light trapping ability and improving photocatalytic performance.

The photocatalytic overall water splitting performance was assessed in a catalysis system under simulated sunlight irradiation without sacrificial agents (Fig. 3a). Initially, TiO_2 hollow nanoshells exhibited low gas production due to rapid charge recombination and high overpotential on the surface. However, when Pt or RuO_2 cocatalysts were integrated into the TiO_2 nanoshells, successful H_2 and O_2 evolution from pure water splitting was observed. Particularly, Pt@TiO_2@RuO_2 hollow nanoshells, featuring spatially-separated cocatalysts, demonstrated the most effective photocatalytic water splitting performance. This was evidenced by a stable H_2 generation rate of 50.1 μmol g^{-1} h^{-1} and O_2 evolution rate of 25.1 μmol g^{-1} h^{-1}, maintaining a near stoichiometric ratio of 2:1. Results presented in Table S1 (Supporting information) show that these hollow nanoshells exhibit competitive photocatalytic activity for overall water splitting when compared to related samples in literature. The stability of Pt@TiO_2@RuO_2 hollow nanoshells was assessed through a cycle test of overall water splitting (Fig. S2 in Supporting information). The catalyst exhibited consistent H_2 and O_2 evolution under simulated sunlight in each cycle, and nearly 90% of the initial activity was maintained after 24 h, making Pt@TiO_2@RuO_2 hollow nanoshells a promising candidate for practical applications. The experiments highlighted the importance of cocatalysts in enhancing charge separation for water splitting, as well as the role of dielectric Mie resonance in hollow nanoshells for improved light trapping. Solar energy and seawater are abundant resources, making seawater an ideal industrial-grade resource for hydrogen and oxygen production through photocatalysis [43]. However, the performance of photocatalytic seawater splitting can be affected by various factors such as solution pH, cations, anions, and competitive reactions due to the thermodynamic favorability of certain species over water molecules [44]. This work focuses on photocatalytic pure water splitting and further research need to be conducted to clarify the influence of water quality on the photo-

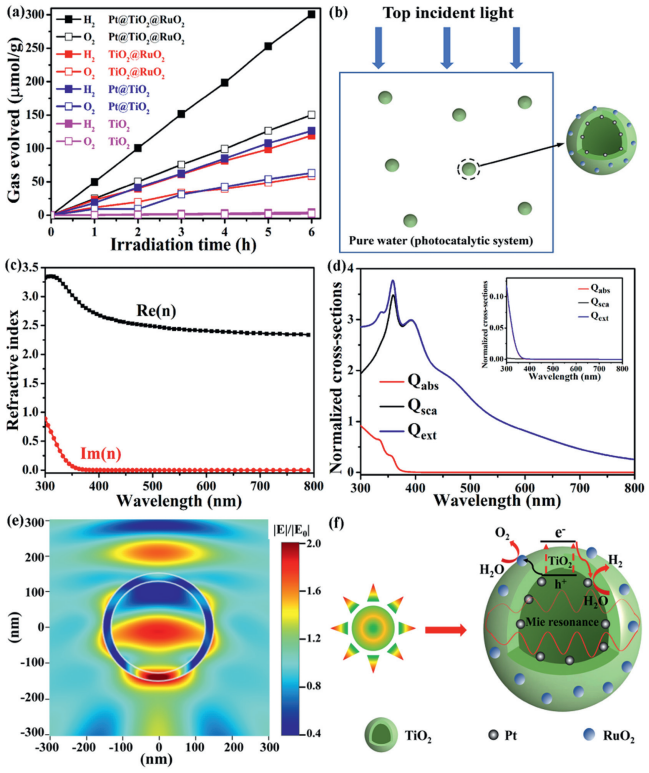

Fig. 3. (a) Photocatalytic overall water splitting over different catalysts under simulated sunlight irradiation. (b) Schematic illustration of photocatalytic water splitting with Pt@TiO_2@RuO_2 hollow nanoshells as the catalyst. (c) Refractive index of TiO_2 in the wavelength range of 300–800 nm. (d) Simulated cross-section of absorption, scattering and extinction of TiO_2 hollow nanoshells (inner diameter of 260 nm and shell thickness of 23 nm) and TiO_2 nanoparticles (inset). (e) Optical field profiles (electric field amplitude) for dielectric Mie resonance in TiO_2 hollow nanoshells at 359 nm. (f) Schematic illustration of Mie resonance, light utilization, and charge separation in Pt@TiO_2@RuO_2 hollow nanoshells for photocatalytic overall water splitting.

catalytic water decomposition performance. Additionally, theoretical calculation based on Mie theory was used to analyze the optical properties and electric field distribution in hollow nanoshells. The simulation model depicted in Fig. 3b illustrated the efficient capture of incident light by suspended nanoshells in water, leading to the generation of photo-induced charge carriers through dielectric Mie resonance. The refractive index of TiO_2, as shown in Fig. 3c, considered the absorption properties in the ultraviolet region by incorporating the imaginary part of the refractive index. Fig. 3d illustrated the simulated absorption, scattering and extinction cross-section of TiO_2 hollow nanoshells and nanoparticles (inset). TiO_2 hollow nanoshells exhibited significant absorption below 400 nm, with no absorption observed in the visible light region. The scattering spectrum of TiO_2 hollow nanoshells displayed two peaks at 359 nm and 393 nm, along with a broad scattering band from 400 nm to 800 nm. The extinction spectrum of TiO_2 hollow nanoshells was a combination of the absorption and scattering spectra. When compared to TiO_2 nanoshells, TiO_2 nanoparticles with a crystalline size of 7 nm showed absorption below 400 nm but weak scattering in the 300–800 nm range. The TiO_2 nanoparticles were actually derived from the structural fragmentation of TiO_2 hollow nanoshells through grinding in an agate mortar. The size of the TiO_2 nanoparticles was identical to that of TiO_2 hollow nanoshells. Based on the XRD results (Fig. 2a), the crystalline size of the anatase TiO_2 nanoparticles was determined to be 7.0 nm using Scherrer's equation. Consequently, the size of the TiO_2 nanoparticles was set at 7 nm for the simulated calculations. The scattered light within the absorption range of TiO_2 can excite nearby nanoparticles to generate charge carriers. In Fig. 3e, the electric near-field distribution around the TiO_2 hollow nanoshells at a resonance wavelength of 359 nm was simulated using the finite-difference time-domain (FDTD) method. The incident light was directed along the z-axis above the nanoshell. The electric-field enhancement, defined as $|E|/|E_0|$ (where E_0 is the incident field amplitude), showed a significant increase in electric field intensity around the nanoshell, reaching a value of 2.0. This localized electric field within the nanoshell enhances light trapping efficiency, as absorbed power is proportional to the square of the electric field [45,46]. Given that anatase TiO_2 has a bandgap of 3.2 eV and strongly absorbs UV light below 387 nm, the enhanced electric field at 359 nm can further excite TiO_2 to generate more electrons from the valence band to the conduction band, resulting in stronger photoluminescence emission, higher photocurrent response, and better photocatalytic activity. Finally, a mechanism was proposed for photocatalytic overall water splitting using Pt@TiO_2@RuO_2 hollow nanoshells, considering dielectric Mie resonance, light utilization, and charge separation (Fig. 3f). When exposed to simulated sunlight, electrons moved from the valence band to the conduction band of TiO_2. The confined nanoshells allowed incident light to travel around, enhancing the near electric field due to dielectric Mie resonance at 359 nm. This further excited the TiO_2 semiconductors, increasing the production of charge carriers and improving light utilization efficiency. Additionally, photo-induced electrons migrated to inner Pt sites for water reduction, while photo-induced holes transferred to RuO_2 sites for water oxidation, enhancing the hydrogen and oxygen evolution rate through spatial charge separation.

In summary, this study effectively illustrated the dual functionality of designed Pt@TiO_2@RuO_2 hollow nanoshells in boosting photocatalytic overall water splitting through dielectric Mie resonance and spatial separation of cocatalysts. Various methodologies, such as template synthesis, surface modification, and ion-exchange, were employed to fabricate TiO_2 hollow nanoshells with Pt nanoparticles inside and RuO_2 nanoparticles outside in a controllable manner. Experimental techniques including photoluminescence emission, photocurrent measurements, and hydrogen production, along with theoretical simulations using Mie theory, confirmed the presence of dielectric Mie resonance in the hollow nanoshells. The resonant scattering at 359 nm facilitated efficient light absorption by enhancing electric-field energy transfer. The spatial separation of cocatalysts promoted charge migration, leading to high rates of hydrogen and oxygen evolution during water splitting. Overall, the discovery of dielectric Mie resonance in nanoshells presents a novel approach to improve light absorption and enhance solar-to-chemical conversion.

Declaration of competing interest

The authors declare that they have no known competing financial interests or personal relationships that could have appeared to influence the work reported in this paper.

CRediT authorship contribution statement

Xiaxi Yao: Writing – original draft, Visualization, Project administration, Investigation, Funding acquisition, Data curation, Conceptualization. **Xiuli Hu:** Resources, Investigation. **Fangcheng Huang:** Writing – review & editing, Software, Methodology. **Xuhong Wang:** Resources, Investigation. **Xuekun Hong:** Writing – review & editing, Supervision, Funding acquisition, Conceptualization. **Dawei Wang:** Writing – review & editing, Supervision, Project administration, Conceptualization.

Acknowledgments

This work was supported by the National Natural Science Foundation of China (Nos. 51702023, 62274017), Natural Science Foundation of Jiangsu Province (No. BK20231224), and China Postdoctoral Science Foundation (No. 2022M711138).

Supplementary materials

Supplementary material associated with this article can be found, in the online version, at doi:10.1016/j.cclet.2024.110192.

References

[1] L. Wang, X. Zheng, L. Chen, Y. Xiong, H. Xu, Angew. Chem. Int. Ed. 57 (2018) 3454–3458.
[2] X. Chen, J. Wang, Y. Chai, Z. Zhang, Y. Zhu, Adv. Mater. 33 (2021) 2007479.
[3] D. Dai, X. Liang, B. Zhang, et al., Adv. Sci. 9 (2022) 2105299.
[4] S. Cao, J. Low, J. Yu, M. Jaroniec, Adv. Mater. 27 (2015) 2150–2176.
[5] Y. Ma, X. Wang, Y. Jia, et al., Chem. Rev. 114 (2014) 9987–10043.
[6] X. Zhang, T. Peng, S. Song, J. Mater. Chem. A 4 (2016) 2365–2402.
[7] R. Shi, Y. Cao, Y. Bao, et al., Adv. Mater. 29 (2017) 1700803.
[8] W. Hou, S. Cronin, Adv. Funct. Mater. 23 (2013) 1612–1619.
[9] G. Fu, M. Jiang, J. Liu, et al., Nano Lett. 21 (2021) 8824–8830.
[10] J. Yin, Y. Zang, C. Yue, et al., Phys. Chem. Chem. Phys. 15 (2013) 16874–16882.
[11] J. Grandidier, D. Callahan, J. Munday, H. Atwater, Adv. Mater. 23 (2011) 1272–1276.
[12] S. Liu, B. Shi, W. Sun, H. Li, J. Yang, Appl. Phys. Express. 11 (2018) 082201.
[13] M. Xiao, H. Chen, T. Ming, L. Shao, J. Wang, ACS Nano 4 (2010) 6565–6572.
[14] W. Ji, L. Li, W. Song, et al., Angew. Chem. Int. Ed. 58 (2019) 14452–14456.
[15] Y. Yao, J. Yao, V. Narasimhan, et al., Nat. Commun. 3 (2012) 664.
[16] A. Kuznetsov, A. Miroshnichenko, M. Brongersma, Y. Kivshar, B. Luk'yanchuk, Science 354 (2016) aag2472.
[17] X. Yao, X. Hong, Y. Liu, Responsive Mater. 1 (2023) e20230019.
[18] K. Chen, L. Wang, H. Tong, et al., J. Mater. Sci: Mater. Electron. 31 (2020) 17659–17669.
[19] X. Yin, J. Zhai, P. Du, et al., Chem. Eng. J. 439 (2022) 135703.
[20] M. Retsch, M. Schmelzeisen, H. Butt, E. Thomas, Nano Lett. 11 (2011) 1389–1394.
[21] L. Fielding, O. Mykhaylyk, A. Schmid, et al., Chem. Mater. 26 (2014) 1270–1277.
[22] S. Kim, V. Hwang, S. Lee, et al., Small 15 (2019) 1900931.
[23] X. Yao, Y. Bai, Y. Lee, et al., J. Mater. Chem. C 7 (2019) 14080–14087.
[24] X. Yao, X. Hu, Y. Cui, et al., Chin. Chem. Lett. 32 (2021) 750–754.
[25] X. Yao, X. Hu, W. Zhang, et al., Appl. Catal. B 276 (2020) 119153.
[26] H. Yang, C. Sun, S. Qiao, et al., Nature 453 (2008) 638–641.
[27] Q. Xu, L. Zhang, B. Cheng, J. Fan, J. Yu, Chem 6 (2020) 1543–1559.
[28] H. Tada, T. Mitsui, T. Kiyonaga, T. Akita, K. Tanaka, Nat. Mater. 5 (2006) 782–786.
[29] J. Ran, J. Zhang, J. Yu, M. Jaroniec, S. Qiao, Chem. Soc. Rev. 43 (2014) 7787–7812.
[30] J. Feng, F. Lv, W. Zhang, et al., Adv. Mater. 29 (2017) 1703798.
[31] S. Feng, K. Li, P. Hu, et al., ACS Nano 17 (2023) 23152–23159.
[32] D. Zhao, Y. Wei, J. Xiong, C. Gao, D. Wang, Adv. Funct. Mater. 33 (2023) 2300681.
[33] X. Yao, T. Liu, X. Liu, L. Lu, Chem. Eng. J. 255 (2014) 28–39.
[34] X. Yao, X. Hu, Y. Liu, et al., Chemosphere 261 (2020) 127759.
[35] Y. Liu, J. Li, B. Zhou, et al., Environ. Chem. Lett. 7 (2009) 363–368.
[36] N. Zhang, C. Han, Y. Xu, et al., Nat. Photonics 10 (2016) 473–482.
[37] H. Lv, S. Wang, J. Li, et al., Appl. Surf. Sci. 514 (2020) 145943.
[38] J. Li, S. Cushing, F. Meng, et al., Nat. Photonics 9 (2015) 601–607.
[39] S. Cushing, N. Wu, J. Phys. Chem. Lett. 7 (2016) 666–675.
[40] A. Dakshinamurthy, T. Das, P. Ilaiyaraja, C. Sudakar, Front. Mater. 6 (2019) 282.
[41] T. Das, P. Ilaiyaraja, C. Sudakar, ACS Appl. Energy Mater. 1 (2018) 765–774.
[42] F. Li, L. Sun, Y. Liu, et al., J. Hazard. Mater. 400 (2020) 123246.
[43] V. Dang, T. Nguyen, M. Le, et al., Chem. Eng. J. 484 (2024) 149213.
[44] S. Crawford, E. Thimsen, P. Biswas, J. Electrochem. Soc. 156 (2009) H346–H351.
[45] V. Ferry, A. Polman, H. Atwater, ACS Nano 5 (2011) 10055–10064.
[46] H. Duan, Y. Xuan, Appl. Energy. 114 (2014) 22–29.